Compact Beam-Steerable Antenna Array with Two Passive Parasitic Elements for 5G Mobile Terminals at 28 GHz

Zhang, Shuai; Syrytsin, Igor A.; Pedersen, Gert F.

Published in:
I E E E Transactions on Antennas and Propagation

DOI (link to publication from Publisher):
10.1109/TAP.2018.2854167

Publication date:
2018

Document Version
Accepted author manuscript, peer reviewed version

This article has been accepted for publication in a future issue of this journal, but has not been fully edited. Content may change prior to final publication. Citation information: DOI 10.1109/TAP.2018.2854167, IEEE Transactions on Antennas and Propagation

Compact Beam-Steerable Antenna Array with Two Passive Parasitic Elements for 5G Mobile Terminals at 28 GHz

Shuai Zhang, Igor Syrytsin and Gert Frølund Pedersen, *Senior Member*, *IEEE*

***Abstract*—A compact beam-steerable antenna array is proposed for 28 GHz mobile terminals. The proposed array consists of one active element and two passive parasitic elements. Two switches are utilized in the design instead of phase shifters. Each parasitic element can be terminated with short-circuited transmission lines of different lengths via one switch. By controlling the two switches, different reactive impedance is loaded on two parasitic elements. The radiation pattern of the active element can be scattered into different directions by two parasitic elements. The switching loss is studied, where two switches with 2.8 dB loss cause less than 1.82 dB loss for the whole array. The small array locations on the chassis are also investigated. The designed array is smaller than 0.81 wavelength, and covers the band of 28-29 GHz with the scan angle ≥ ±90°. By placing two arrays on each long chassis edge, 360° beam steering can be realized. Surface currents on the chassis are efficiently excited to achieve high gain with the small array. Measurements are carried out and align well with simulations. In practical applications, several small arrays can be implemented on the metal back cover and around a cellphone to combat users' mobility.**

***Index Terms*— Mobile antenna, beam steerable array, 5G application.**

I. Introduction

RECENTLY, centimeter-wave (cm-wave)/millimeter-wave (mm-wave) technologies have become very promising candidates for the fifth generation (5G) cellular communication systems [1]-[2]. In these systems, beam steerable arrays with high gain have to be applied at both base stations and user terminals in order to overcome the path loss. A phased array with hybrid analog phase shifters and digital beamforming is one popular way to realize the beam-steerable array [3]-[4], which is very suitable for base stations. At base stations, there is lots of space to implement large phased arrays with high gain, narrow beam, low sidelobe, wide scan angle and so on. The power supply at base stations also allows the usage of a large number of phased array elements with phase shifters, which are lossy at cm-/mm-wave frequencies. Although digital beamformers are expensive currently, they can still be applied to base stations.

This work was supported by the InnovationsFonden project of "RANGE", and also partially supported by Aalborg University Young Talent Program.

Shuai Zhang, Igor Syrytsin and Gert Frølund Pedersen are with the Antennas, Propagation and Millimeter-wave Systems section at the Department of Electronic Systems, Aalborg University, Denmark (email: sz@es.aau.dk).

However, in mobile terminals, there is very limited space left for 5G arrays after accommodating 2G, 3G and 4G antenna systems. The only power supply in a cellphone is a small battery. Beam-steerable arrays in mobile terminals can also be many other types of arrays besides phased arrays. Due to the mobility of terminal users, there are some new challenges and requirements on the array designs: firstly, the user blockage [5]-[6] (e.g. by hands, body and so on) at cm-/mm-wave frequencies is severe. Different holding gesture may block the scanned beam of an array. As one solution, the arrays have to be designed to be very compact, so that many small arrays can be implemented around a phone to overcome the user blockage. Secondly, the small array should be able to realize beam steering with high gain. Generally, the gain is proportional to the aperture of an antenna. It is challenging to design small arrays with high gain. Moreover, since the orientation of a phone is random, the array should also own large scan angle/coverage to catch the strongest clusters in channel. Finally, as mentioned above, the loss of a conventional phased array with phase shifters in cm-/mm-wave bands is still high currently. Amplifiers can compensate the loss. However, the loss will also lead to the temperature increases. How to decrease the cumulated temperature is still an issue for mobile handsets. Furthermore, in a handset there will be more than one 5G beam steerable arrays. Applying amplifiers to compensate the high loss of all the arrays with phase shifters will shorten the battery life. It is highly preferred if the mobile terminal arrays can scan the beam in a low-cost (or low-loss) way. Therefore, 5G beam-steerable antenna arrays in mobile terminals should have a compact size, the ability of beam steering with high gain, large beam-steering angle/coverage in space, and low cost for beam-steering control.

In recent years, some works have been carried out to design beam-steerable arrays for mobile devices at cm-/mm-wave frequencies. Different phased arrays have been proposed in [7]-[9]. To evaluate the coverage performance of a phased array, the metric of coverage efficiency has been introduced in [10]. A 3D-scan phased array has been designed in [11] in order to enlarge the coverage efficiency, but the array is not planar. To ease the fabrication and keep the 3D-scan property, in [12] a planar 3D-scan phased array has been reported. However, the arrays in [7]-[12] are still the phased arrays with phase shifters. Beamforming networks (e.g., Butler matrix [13]) or lenses (e.g., Rotman [15]-[16]) can be utilized to achieve multi-beams by switching among different feeding ports. And switches are required in these methods. However, the beamforming

This article has been accepted for publication in a future issue of this journal, but has not been fully edited. Content may change prior to final publication. Citation information: DOI 10.1109/TAP.2018.2854167, IEEE Transactions on Antennas and Propagation

networks or lenses are big and occupy lots of space. It will be very challenging if several sub-arrays are implemented in a handset. Furthermore, the scan angle of arrays with beamforming networks or lenses are typically less than ± 60º. Directional antennas have been placed around a mobile terminal to form an array in [16]-[17]. The beam steering is realized by switching the antenna elements pointing in different directions. However, placing some beam steerable arrays around a phone is different from allocating directional antenna elements around a handset. The former one can combat user's blockage, but the latter one cannot. Arrays with parasitic elements (ESPAR, Electronically steerable passive array radiator) have been widely studied [18]-[20]. By loading different reactive impedance on parasitic elements, the array can scan the beam to different directions with only one active element. However, the previous works in [18]-[20] were designed for sub 6 GHz instead of high frequencies and not for mobile terminals either. The insertion loss of commercialized low-loss inductors and capacitors are around 0.5-2 dB (or even worse) in cm-/mm-wave bands, and not all the inductance and capacitance values are available in the market. Moreover, due to the limited space in mobile handsets, the ESPAR array with one active element and two passive elements is a very good candidate. However, the gain of this type of array is not high enough for mobile terminals, which is typically suggested to be over 7 dBi.

The objective of this paper is to design a beam-steerable array with a compact size, low-cost beam-steering control, high gain, and large steering angles. A compact beam-steerable antenna array will be proposed for 5G mobile terminals at 28 GHz. The array consists of one active element and two passive parasitic elements. Reactive impedance loaded on parasitic elements is realized by short-circuited or open-circuited transmission lines of different lengths. Two switches will be utilized in this design to realize the beam steering. Ideal switches will be applied to the antenna design. The impacts of switch loss will also be analyzed. The length of the whole array is less than 0.81 wavelength of the central operating frequency of 28.5 GHz. The designed array covers the band of 28-29 GHz. The scan angle is larger than ±90º. By placing two compact arrays on each long edge of the chassis, 360º beam steering can be achieved. The surface currents on the metal back cover of a mobile terminal will be utilized to obtain high gain for the small array. The proposed concept will also be applied to planar array designs. Measurements will be carried out to verify the simulations. In practical applications, several small arrays can be implemented around a mobile terminal and on the metal back cover of a full-screen phone.

The novelties of this work are as follows: 1. Propose a low-cost (or low-loss) method to realize the beam steering for a compact 5G mobile terminal array; 2. By efficiently exciting surface currents on the metal back cover of a handset, high gain can be realized at different scan angles by a compact non-planar array (0.81 wavelength long) or a compact planar array (about 1 wavelength long); 3. The proposed arrays can reach the scan angle of larger than ±90º.

The design procedure or the organization of this paper is addressed in the following: in Section II, the mechanism of the proposed method for beam steering will be introduced. As the first example, a compact non-planar beam-steerable antenna array with parasitic elements will be designed for 5G mobile terminals in Section III, where the array configuration, performance and loss will be studied. Section IV will investigate how the performance changes with the dimensions and the location of the array (in Section III). A planar array with parasitic elements will be proposed in Section V as the second example. In Section VI, experiments will be carried out to verify the simulations. Finally, conclusions will be given in Section VII.

II. Proposed Technique of Beam Steering with Two Passive Parasitic Elements

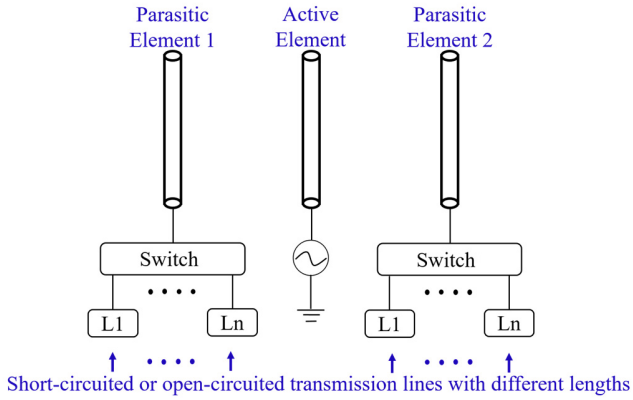

Fig. 1. Proposed technique of beam steering with two passive parasitic elements terminated with short-circuited or open-circuited transmission lines of different lengths.

The sketch of the proposed method for beam steering is shown in Fig. 1. In this method, there are two passive parasitic antenna elements and one active element, which forms a small linear array. In order to make the passive elements efficiently scatter the field, the array element distance is suggested to be less than half wavelength of the central operating frequency. The end of each parasitic element is connected to the input of a switch. And each output of the switch is terminated with a short-circuited or open-circuited transmission line of different lengths. The reactive impedance of the short-circuited or open-circuited transmission line is calculated by (1) and (2), respectively:

$$Z_{short\text{-}circuit} = jZ_o tan(\beta L) \quad (1)$$

$$Z_{open\text{-}circuit} = -jZ_o cot(\beta L) \quad (2)$$

where Z_o is the characteristic impedance of the transmission line, β is the propagation constant, and L is the length of the transmission line. By controlling the two switches, the reactive impedance loaded on two parasitic elements has many different combinations. In this way, the radiation patterns of the active antenna element can be scattered into different directions.

At cm-/mm-wave frequencies, the short circuit of a

This article has been accepted for publication in a future issue of this journal, but has not been fully edited. Content may change prior to final publication. Citation information: DOI 10.1109/TAP.2018.2854167, IEEE Transactions on Antennas and Propagation

transmission line is easier to realize than the open circuit. From our studies, applying open-circuited transmission lines will lead to 0.5 dB higher loss for the whole array system than using the short-circuited. In the following, the short-circuited transmission line will be utilized for the antenna array design.

Furthermore, in practical applications, the short-circuited transmission lines, switches and antenna array elements will be integrated together to form the Antenna-in-Package [21]. In this way, the loss can be further reduced and the system will be more reliable as well.

III. Compact Beam-Steerable Antenna Array with Parasitic Elements for 5G Mobile Terminals

A. Antenna Configuration

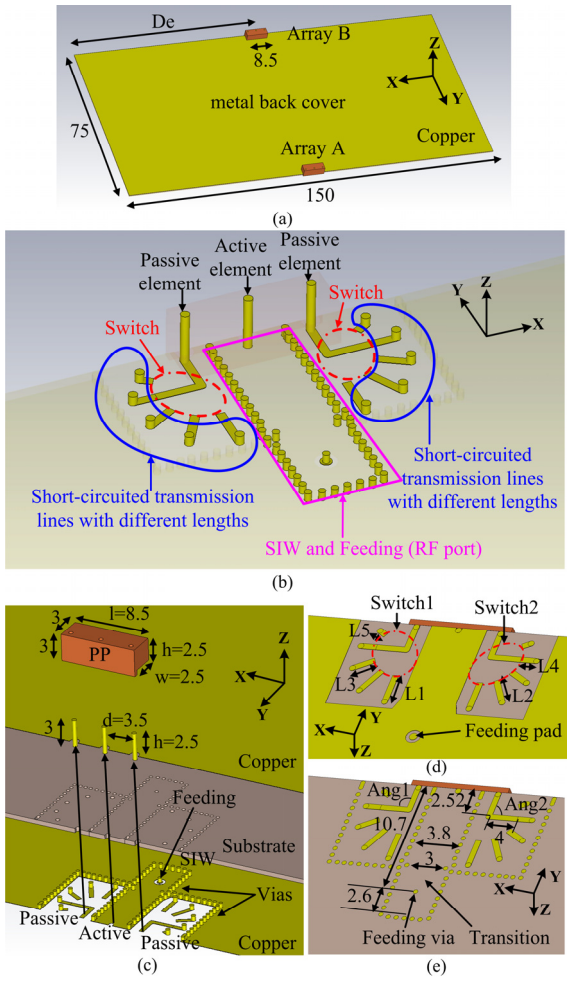

Fig. 2. Geometries of the proposed beam-steerable array with two passive parasitic elements terminated by the short-circuited transmission lines of different lengths: (a) 3-D view, (b) the general view of different major parts in one array with surface copper, substrate and PP dielectric block hidden, (c) 3-D exploded view, (d) back view, and (e) back view with surface copper hidden. (Unit: mm)

The geometries of the proposed beam-steerable array with two passive parasitic elements are shown in Fig. 2. In Fig. 2 (a), two beam-steerable arrays (i.e., array A and array B) are placed at the center of each long chassis edge. In practice, many such small arrays will be allocated around and on the metal back cover of a handset. The general view of different major parts in one array are shown in Fig. 2 (b) with surface copper, substrate and Polypropylene (PP) dielectric block hidden. Different major parts are marked in Fig. 2 (b) as well to correspond to the description in Fig. 1. The array consists of three monopoles. One monopole (out of three) is active and fed by substrate integrated waveguide (SIW), which is the only element connected to the RF port. The other two monopoles are passive and connected to the inputs of two switches via microstrip lines. The outputs of each switch are terminated with short-circuited microstrip lines of different lengths. By controlling the two switches, different reactive impedance can be loaded on two passive monopoles. The detailed array configuration is given in Fig. 2 (c)-(e). Fig. 2 (c) illustrates the 3-D exploded view of one array. The array volume is 2.5 × 2.5× 8.5 mm^3. Each array has three monopoles with the inter-element distance of 3.5 mm. The height of each monopole is 2.5 mm. However, the height can be further decreased by some designs, e.g. capacitive loading (add a small circular metal disc on the end of each monopole). The diameter of the monopoles and the width of the microstrip lines are 0.5 mm. Since the polarization of the monopoles is perpendicular to the chassis, strong surface currents can be excited on the metal back cover to enlarge the gain of the small array. A PP block is applied as a supporting material for monopoles. PP is a very low-cost material which is widely used at sub 6 GHz. The electrical properties of PP from 5 GHz to 67 GHz is measured with the material analyzer of SPEAG DAK-TL, which is given in Fig. 3. At 28 GHz, the permittivity and loss tangent is 2.27 and 0.0003, respectively. In Fig. 2 (d), the lengths of 5 short-circuited microstrip lines are L1=2.6 mm, L2=2.3 mm, L3=1.8 mm, L4=1.3 mm, L5=0.7 mm, respectively. By changing Ang1 and Ang2 in Fig. 2 (e), the two passive monopoles can load different reactive impedance on them. The microstrip line (see Fig. 2 (d) and (e)) with Ang1 (or Ang2) = 180º, 150º, 120º, 90º, 60º will connection to L1, L2, L3, L4, L5, respectively. 7 states with different combinations of Ang1 and Ang2 are given in Table I. In addition, an MMPX (coaxial) connector [22] is used to feed the SIW. A small transition is added from MMPX to SIW, as shown in Fig. 2 (d).

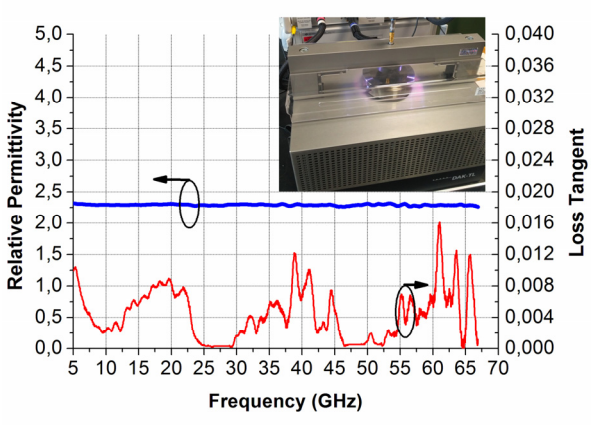

Fig. 3. Measured relative permittivity and loss tangent of Polypropylene.

This article has been accepted for publication in a future issue of this journal, but has not been fully edited. Content may change prior to final publication. Citation information: DOI 10.1109/TAP.2018.2854167, IEEE Transactions on Antennas and Propagation

TABLE I
STATES WITH DIFFERENT COMBINATIONS OF ANG1 AND ANG2

	State A	State B	State C	State D	State E	State F	State G
Ang1	180°	150°	120°	90°	90°	60°	60°
Ang2	60°	60°	90°	90°	120°	150°	180°

B. *Antenna Performance*

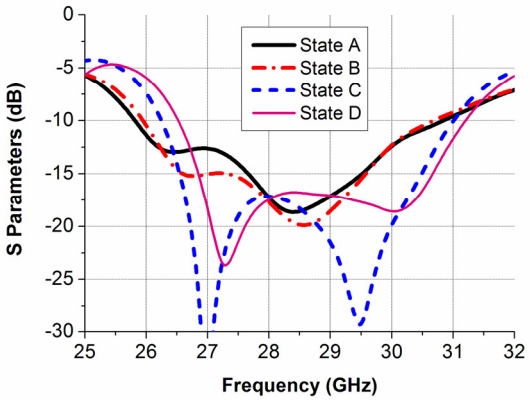

Fig. 4. S parameters of the proposed beam steerable array in different states.

The S parameters of the proposed beam steerable array in different states are given in Fig. 4. Since the antenna array system is symmetric in *yz* plane (see Fig. 2), only the S parameters of the State A, State B, State C, and State D are given. The impedance bandwidth is from 26.5 to 31 GHz with the specification of -10 dB. There are two or three resonances in different states in Fig. 4. These resonances are mainly due to the two parasitic elements. The parasitic element will not only help steer the main beam direction, but also enlarge the impedance bandwidth. The reflection coefficients in different states are sufficient to cover the target band of 28-29 GHz. Furthermore, if two small arrays are placed at two long edges of the chassis (see Fig. 2 (a)), mutual coupling between two arrays is less than -37 dB in all different states.

The simulated 3D radiation patterns of the proposed beam steerable array in different states at 28.5 GHz are shown in Fig. 5. The radiation patterns at the other frequencies of 28-29 GHz are similar to those in Fig. 5. With the 7 states, the array scans the beam from 180° to 360° with high gain. The wide scan angle is mainly caused by the wide beam width of the monopole elements. The far field of the proposed beam steerable array is constructed by the far field of the active element and two coupled parasitic elements. Therefore, the array scan angle is related to the element beam width instead of the long chassis edge. The maximum gain of the array is affected by the surface currents [12] on the chassis. The strength of the surface currents is determined by the element perpendicular polarization as well as the size and shape of the whole metal chassis. If the proposed compact array works as a conventional phased array and in the same condition to that in Fig. 2, it will also have wide scan angle and high gain. Therefore, this is a general way of realizing wide scan angle and high gain with a small array.

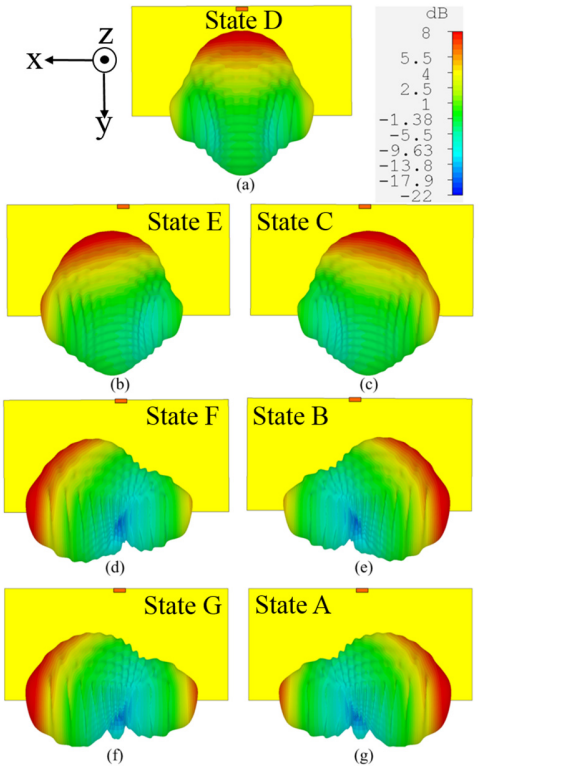

Fig. 5. Simulated 3D radiation patterns of the proposed beam steerable array in different states at 28.5 GHz.

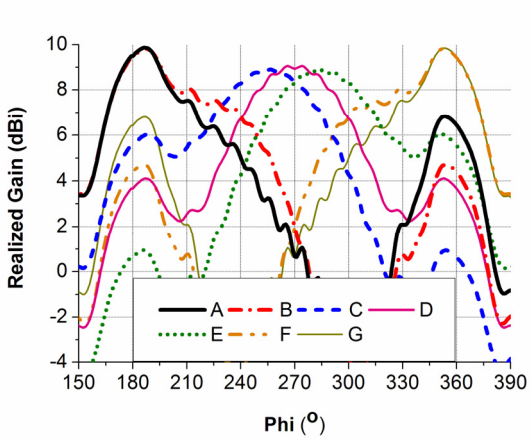

Fig. 6. Simulated radiation patterns of the proposed beam steerable array in different states in the plane of θ= 72° at 28.5 GHz.

To better observe the beam-scan property, the radiation patterns of the proposed array in the plane of θ= 72° are shown in Fig. 6. The gain is over 7.5 dBi from around 170° to 370°. State B (or State F) is a little similar to State A (or State G). However, State B (or State F) can still improve the gain at 220° (or 320°) by 1-1.5 dBi. Furthermore, each passive monopole is terminated with one of 5 short-circuited microstrip lines. In the applications, one 1-input and 4-output (1P4T) reflective switch can be used for each passive monopole. The 4 outputs can be connected to 4 short-circuited microstrip lines, and the last reactive impedance can be realized by opening all the 4 outputs. Typically, switches in 28 GHz band in the market have even number outputs. The loss of switch increases with the number

This article has been accepted for publication in a future issue of this journal, but has not been fully edited. Content may change prior to final publication. Citation information: DOI 10.1109/TAP.2018.2854167, IEEE Transactions on Antennas and Propagation

of outputs. Whether the State B and State F are included will not change the output port number. In addition, the radiation patterns in Fig. 5 and Fig. 6 are from only one array. If another array is put on the other side of the long chassis edge (see Fig. 2(a)), the scan angle of 0°-360° can be achieved.

The realized gain of the proposed array at different frequencies is presented in Fig. 7. The realized gain in State C and D (see Fig. 7) is stable over a wide frequency range, while the gain of State A and B varies a little with frequencies. The gain in different states is over 9 dBi and over 7.5 dBi in the band of 28-29 GHz and 27.5-29.5 GHz, respectively. Since the antenna elements applied here are simple monopoles, it is possible to further improve the gain bandwidth of State A and B by designing array elements and array structures in the future work. In addition, please note that the length of one small array is only 8.5 mm, which is less than 0.81 wavelength. As mentioned above, the high gain with such small an array is mainly due to the utilization of surface currents on the metal cover. Since this small array will be implemented on the metal back cover of a full-screen phone, the array beams will not interact too much with the other phone components.

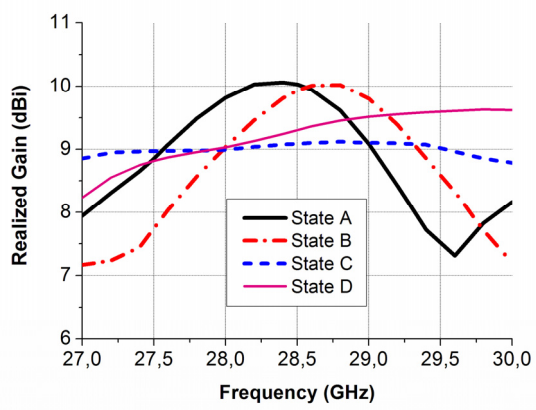

Fig. 7. Simulated realized gain of the proposed beam steerable array in different states at different frequencies.

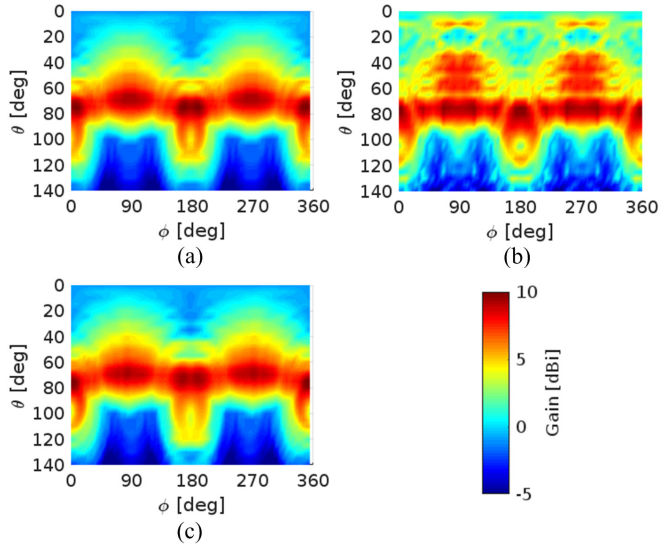

Fig. 8. Total scan pattern at 28.5 GHz: (a) simulation and (b) measurement with two arrays on the center of two long chassis edges, and (c) simulation with two arrays off center (48 mm away from the short chassis edge, De=48 mm).

The total scan pattern [10] with two arrays on the center of two long chassis edges (i.e., array A and array B in Fig. 2 (a)) is shown in Fig. 8 (a). 360° coverage in ϕ with high gain can be observed clearly. Coverage efficiency is defined as [10]:

$$Coverage\ Efficiency = \frac{Coverage\ Solid\ Angle}{Maximum\ Solid\ Angle}\Big|_{threshold\ realized\ gain} \quad (3)$$

where the coverage solid angle of the array beam is calculated by the total scan pattern higher than a certain threshold realized gain; the maximum solid angle is 4π steradians if the whole spatial sphere is chosen. The coverage efficiency of the above-mentioned two arrays is shown in Fig. 9, where good coverage can be observed.

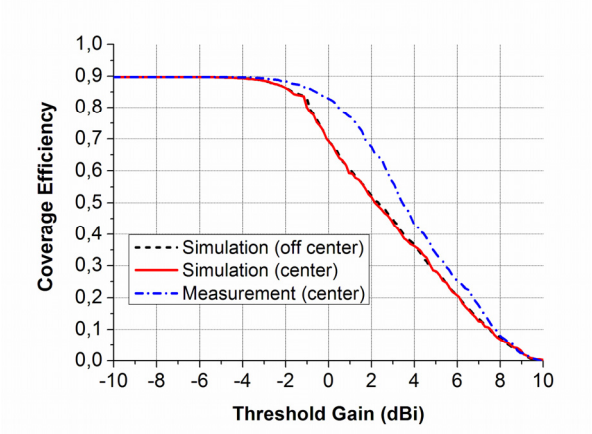

Fig. 9. The simulated and measured coverage efficiency simulated and measured center, simulated edge.

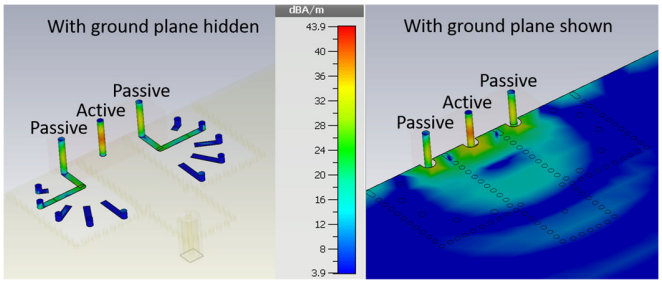

Fig. 10. Current distributions on the three monopoles in State D.

The current distributions on the three monopoles in State D are added in Fig. 10, in order to better understand how to excite the two side monopoles which are connected to the short-circuited microstrip lines. It can be seen that the active monopole induces coupled currents on the passive elements and the connected microstrip lines. The far field of the array is constructed by the far fields of one active and two passive monopole elements.

In addition, as aforementioned, there will be several subarrays distributed around a 5G handset. If phased arrays are applied, each subarray are expected to have 4 elements in order to achieved the high gain (e.g. of over 7 dBi). The length of each phased subarray length will be about 1.5 wavelength. The same number of our proposed beam steerable arrays can be used as subarrays to replace these phased subarrays. The length

This article has been accepted for publication in a future issue of this journal, but has not been fully edited. Content may change prior to final publication. Citation information: DOI 10.1109/TAP.2018.2854167, IEEE Transactions on Antennas and Propagation

of each proposed array with the high gain is less than 0.81 wavelength, which is nearly half of the conventional phased array with 4 elements. One array for both receive and transmit is one of the scenarios for 5G handset antennas, where the proposed arrays can also work in the same way to the conventional phased subarrays.

C. *Analysis of Switch Loss Impacts*

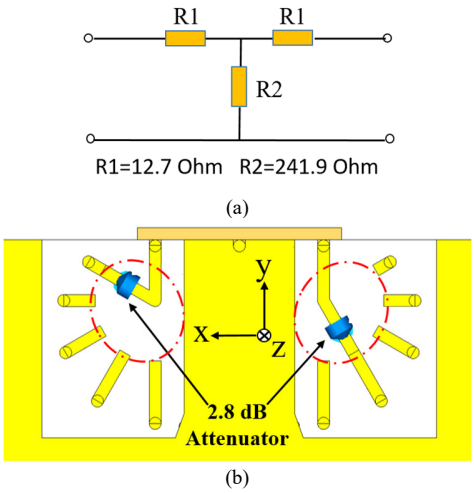

Fig. 11. Switches with loss: (a) attenuator circuit, and (b) the attenuators on the switching parts.

Practical switches have loss. Switch loss increases with the output port number of the switch. Switches have the types of the reflective switches (with de-active ports open or short) and the non-reflective switches (with de-active ports terminated by 50-ohm loads or absorbers). In our design, 1-input and 4-output (1P4T) reflective switches are needed. Commercialized 1P4T reflective and non-reflective switch modules (instead of dies) at 28 GHz can be found in [24] and [25] with the insertion loss of 2.8 dB and 2.4 dB, respectively. The switch model information can be found in the date sheets of [24] and [25]. In addition, practical phase shifters also have loss. The loss of phase shifters increases with the state number (or the Bit number), operating frequencies, and so on. Our proposed array has 7 states (or beams). It is corresponding to 3-Bit phase shifter modules if phase shifters are applied. Commercialized 3-Bit phase shifter modules at 28 GHz are not available in the market now. The insertion loss of commercialized 5-Bit phase shifter modules (instead of dies) at 29-31 GHz is 9 dB [26]. And commercialized 4-Bit phase shifter modules at 8-12 GHz have the insertion loss of 6.5 dB [27]. Currently, a very optimal estimation of commercialized 3-bit phase shifter modules should have the insertion loss of over 6 dB at about 28 GHz. It should be noticed that the above comparison does not tend to claim switch modules are less lossy than phase shifter modules since the loss depends on lots of factors. Instead, we would like to claim that the proposed beam steerable array can utilize two 1P4T reflective switch modules (with the loss of 2.8 dB) to realize the similar number of states (or beams) compared with the conventional phased arrays with 3-Bit phase shifter modules (with the loss of over 6 dB) at 28 GHz.

In order to study the switch loss impact on the array performance, a 2.8 dB attenuator is applied for each of the passive monopoles in the simulations, as shown in Fig. 11. In practical applications, the red circle areas in Fig. 11 (b) can be replaced by 1P4T reflective switches. The 1 input of each switch will be connected to each passive monopole. The 4 outputs can be connected to 4 short-circuited transmission lines (e.g. L2, L3, L4 and L5 in Fig. 2), and the last reactive impedance can be realized by opening all the 4 outputs. Therefore, only 4 short-circuited transmission lines (for each switch) are required if 1P4T reflective switches are applied in practice. In addition, we believe the conclusions will be very similar to utilize a real switch or a 2.8 dB attenuator in this study, since the insertion loss between the input port and each output port is clearly given in the data sheets of the commercialized switch modules (e.g. [24]). Indeed, there may also be some practical impacts if real switches are utilized, for example: 1. the mutual coupling between the short-circuited microstrip lines may change the port isolation of switches. This can be solved by using the short-circuited SIW transmission lines or shielded strip lines. 2. the real switch itself also has a physical length. This physical length may affects the length of each short-circuited transmission line. However, the operating principle is still the same. And the length of each short-circuited transmission line can be adjusted according to the detailed dimension and layout of the switches if we have these information. In the applications, at mm/cm-frequencies, the antennas, switches/phase shifters, and transmission lines are usually integrated into a module instead of being soldering together separately. During the integration, the geometrical information of switches will be available. As the first step, we would like to demonstrate our proposed idea (/concept) and operating principle in this paper. In the very near future, two switches, transmission lines and antennas will be integrated together into a commercialized module, which will be connected to mmWave RFICs.

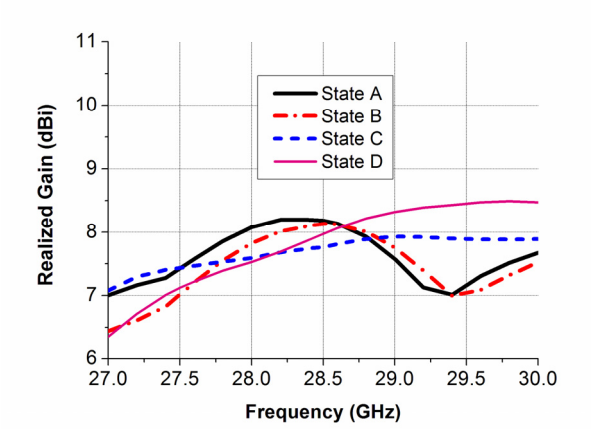

Fig. 12. Simulated realized gain of the proposed array in different states with 2.8 dB loss on the switches.

The realized gain of the proposed array in different states with lossy switches is provided in Fig. 12. Comparing the gain in Fig. 12 with the one in Fig. 7, the loss of the whole array system from two 2.8 dB-loss switches is 1.15-1.82 dB. It can be expected that if the conventional phased array with 3-Bit phase shifter modules the loss will be over 6 dB at 28 GHz. The reasons for the lower loss with the proposed array is that: 1. the short-circuited microstrip lines are connected to passive

This article has been accepted for publication in a future issue of this journal, but has not been fully edited. Content may change prior to final publication. Citation information: DOI 10.1109/TAP.2018.2854167, IEEE Transactions on Antennas and Propagation

monopoles, and the currents on the passive monopoles are just part of the total currents. Fewer currents flowing on switches will lead to less loss; 2. The proposed array can utilize two 1P4T reflective switches with 2.8 dB loss to realize 7 beams or states instead of using 3-Bit phase shifter modules with over 6 dB loss at 28 GHz. Furthermore, it is also noticed that different states in Fig. 12 have different gain loss with the lossy switches. This is because the lossy switch is placed at different locations of the standing-wave currents of the short-circuited microstrip lines with different lengths. By utilizing this property, it is possible to make a tradeoff between the gain loss of different states.

IV. Parametric Studies

In the applications, several proposed arrays will be placed around a mobile terminal. It is important to know how different states are affected by the array dimensions and array location on the metal back cover.

A. Array Inter-Element Distance

The inter-element distance of the array should be less than the half wavelength. In this way, the passive monopoles can efficiently scatter the radiation patterns of the active monopole. The tendency of the gain variation with different element distances in State A and State D is very similar to that in State B and State C, respectively. Therefore, only realized gain of the State A and State D under different element distances are shown in Fig. 13. With the element distance increasing from 3.25 mm to 3.75 mm, the gain of State A (or State B) is lower, while the gain of State D (or State C) is higher. A trade-off between the gain of State A and State D is noticed.

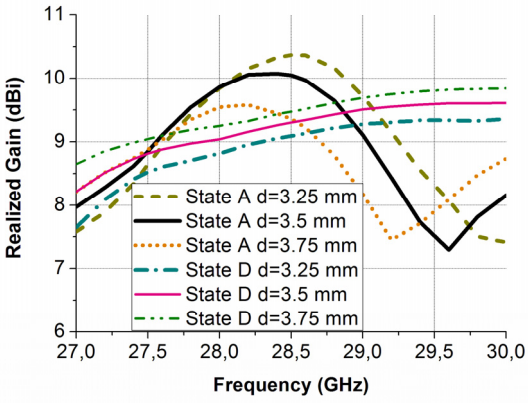

Fig. 13. Realized gain of the State A and State D under different array element distances.

B. Length and Width of Compact Array Dielectric Block

The PP dielectric block will also affect array performance. Similarly to Section IV-A, only the realized gain of the State A and State D are shown in Fig. 14, with different lengths and widths of the PP block. In general, a shorter and narrower block will lead to the higher gain of State A (or State B), but will deteriorate the gain of State D (or State C). However, this tendency is not always well kept. For example, the gain of State D with 2.5 mm is better than that with 3 mm. This property can be utilized to slightly improve the array performance with a smaller array.

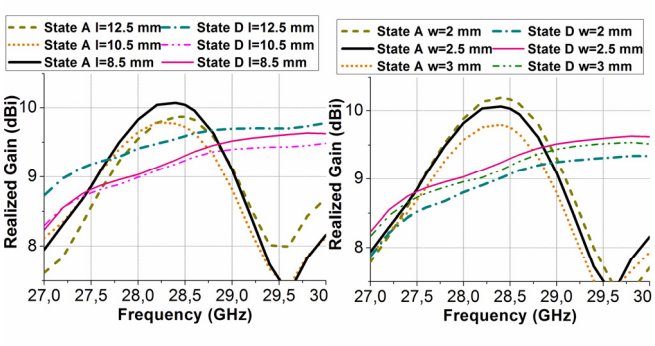

(a) (b)

Fig. 14. Realized gain of the State A and State D: (a) with different lengths of the block, and (b) with different widths of the block.

Based on the parametric studies in Section IV A and B, during the design a tradeoff between the realized gain of different states can be made, so that different states will have similar gain within the target band.

C. Location of the Compact Array on Mobile Chassis

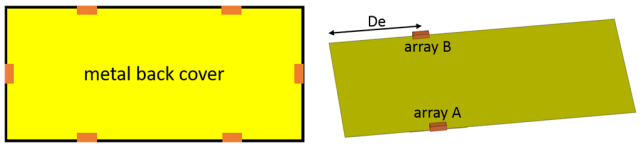

(a) (b)

Fig. 15. Sketch of: (a) distributed small arrays around a mobile terminal in practical applications, and (b) array A and array B under different distances between arrays and short chassis edge (De).

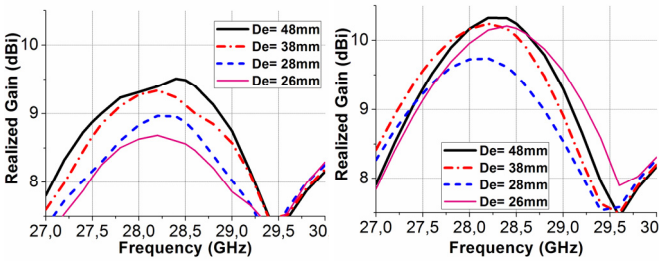

(a) (b)

Fig. 16. Simulated realized gain under different De for: (a) State A, and (b) State G.

The proposed small beam-steerable arrays can be distributed around a handset, as shown in Fig. 15 (a). In this way, user tissue blockage in 28 GHz bands can be combatted. In the studies above, the arrays are allocated at the center of two long chassis edges. It is necessary to know how the small array performance changes with the array-(short) edge distance (De). By varying De, the State C, State D, and State E seldom change. State A and State B have the similar tendency, while State F and State G also experience a similar trend. Hence, only the gain of State A and State G is investigated here. Fig. 16 shows the realized gain under different De (in Fig. 15 (b)) for State A, and State G. The gain of State A for De= 26 mm (nearly the worst case) is around 1.4 dB lower than that for De= 0 mm (in Fig. 7). As the array moves in the +x direction (see Fig. 2), the gain of State A gets lower as expected. The gain of State G is

This article has been accepted for publication in a future issue of this journal, but has not been fully edited. Content may change prior to final publication. Citation information: DOI 10.1109/TAP.2018.2854167, IEEE Transactions on Antennas and Propagation

kept more or less the same except for the position of De=28 mm where the gain drop occurs. The reason for this gain drop is mainly due to surface current (or wave) superposition [12]. At some locations, the surface currents in the –x direction are out of phase with those reflected by end of the long edge in the +x direction. Indeed, we can also choose some locations satisfying the in-phase superposition to optimize the gain. Finally, it should be emphasized that the proposed antenna can always realize beam steering when placed at different locations around the chassis edge. Depending on the array locations, the realized gain in some states may decreases less than 1.5 dBi (in the worst case of De= 26 mm) compared to the gain with the array on the center of the long chassis edge. This variation is still within the acceptable range. The tendancies are still consistant in the different states.

The small arrays for De=48 mm are illustrated in Fig. 15 (b), which is a most likely location for applications. The total scan pattern and coverage efficiency of the array, in this case, are calculated and shown in Fig. 8 (c) and Fig. 9, respectively. It is noticed that the arrays for De= 48 mm and on the center of the long edge have very similar coverage performance, which is a desired feature.

V. Planar Array Design with Parasitic Elements

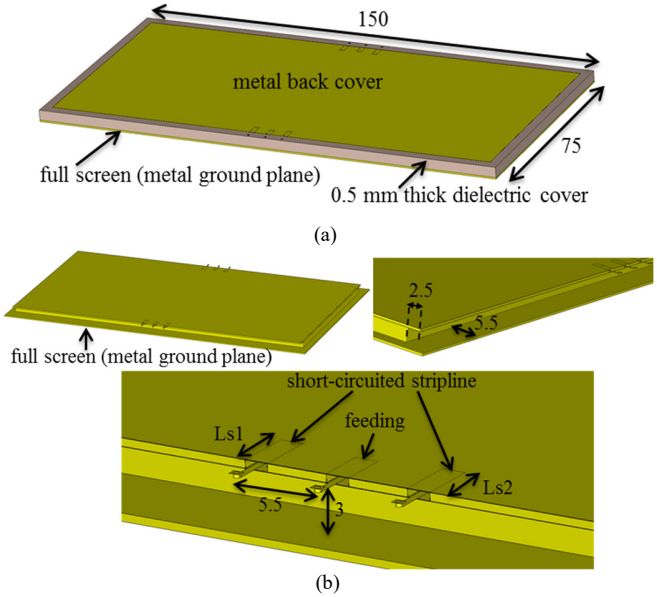

Fig. 17. Geometries of the proposed planar array with two passive parasitic elements terminated by the short-circuited strip lines of different lengths: (a) back view, (b) back view with dielectric cover hidden. (Unit: mm)

The design introduced in Fig. 2 is very convenient to be integrated as one package or module that includes the antenna array, short-circuited transmission lines, and switches. If a planar array is required, the proposed method can also be utilized. Strong surface currents (for high gain realization) can also be excited by some planar antennas, such as planar monopoles (placed at the edge of a metal chassis), slot antennas [12], and so on. If slots are applied, it is recommended to bend a slot from the straight to the U-shape, so that the beam width of each slot antenna in horizontal plane can be broader. Due to the page length limitation, the design with slot antennas will not be discussed here. In this section, as one design example, we will use planar monopoles.

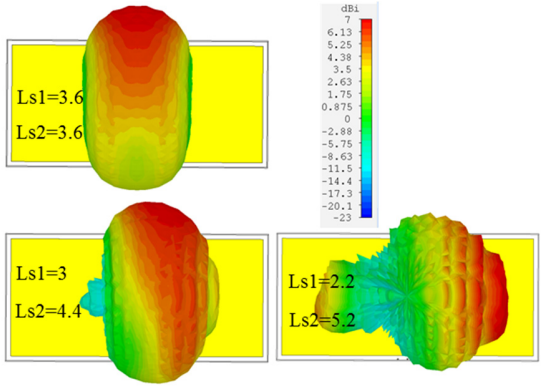

Fig. 18. Simulated 3D radiation patterns of the planar array in different states at 27 GHz.

The design is shown in Fig. 17. The active element and parasitic elements are planar monopoles integrated to the metal back cover of a full-screen phone. The dielectric substrate and frame in Fig. 17 (a) is 0.5 mm thick and made of Rogers 5880 with the permittivity of 2.2. In [23], the metal ground plane for the full screen (see Fig. 17 (b)) has served as one part of a back cavity to design an endfire array. In order to make the antenna radiate only in the back cover direction, the metal ground plane for the full screen is used as a reflector in this paper, which is 3 mm away from monopoles. The active element is fed by a strip line and the parasitic elements are connected to short-circuited strip lines. To simplify the model, the lengths of two short-circuited strip lines are set as Ls1 and Ls2, respectively.

The planar array covers the band of 26-28 GHz with the reflective coefficient of better than -10 dB in different states. The simulated 3D radiation patterns of the planar array in different states are given in Fig. 18 at 27 GHz. Please note there are 5 states in total to cover the 180° scan angle. Since the radiation patterns are symmetrical, only 3 states are shown Fig. 18. The realized gain for different states within 26-28 GHz is from 7 dBi to 9.3 dBi, which is good enough for the application of 5G mobile terminals.

VI. Experiments and Discussions

The proposed beam-steerable array with parasitic elements has been fabricated. The prototypes of the antenna in different states are shown in Fig. 19 (a). The compact array dimensions are observed clearly. The antennas are fed by MMPX connectors. In all the measurements, a transition cable from an MMPX connector to a K connector (which is compatible with an SMA connector) is applied. The loss of MMPX connector and transition cable is about 2.2 dB in total, which has been excluded from all the measured data. Please note that the prototypes here are mainly used to verify the simulations instead of showing the final realistic scenario. Real switches are not used in the prototype, because it is very challenging to control the accuracy when soldering the switch with each

This article has been accepted for publication in a future issue of this journal, but has not been fully edited. Content may change prior to final publication. Citation information: DOI 10.1109/TAP.2018.2854167, IEEE Transactions on Antennas and Propagation

microstrip lines manually. The lengths of 5 short-circuited microstrip lines are L1=2.6 mm, L2=2.3 mm, L3=1.8 mm, L4=1.3 mm, L5=0.7 mm, respectively. The differences are small and manually soldering may change the length of the microstrip lines. As mentioned above, at mm/cm-frequencies, the antennas, switches, and transmission lines will be integrated into a module in the near future, so that the accuracy can be well controlled in practical applications.

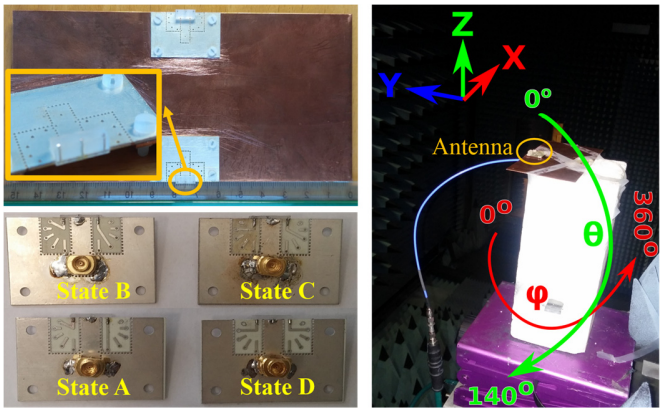

(a) (b)

Fig. 19. (a) Prototypes of the proposed antenna, and (b) measurement setups in an anechoic chamber.

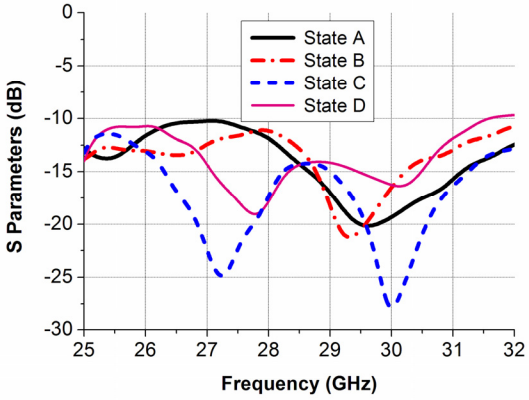

Fig. 20. Measured S parameters in different states.

The S parameters of the prototypes are measured and given in Fig. 20. The array can still cover the target band of 28 GHz to 29 GHz with the specification of -10 dB. Compared with the results in Fig. 4, the measured S parameters slightly shift to higher frequencies, but still align well with the simulations.

The radiation patterns of the proposed arrays are measured in an anechoic chamber, where the measurement setups are illustrated in Fig. 19 (b). A standard horn antenna for the gain calibration has been utilized before the measurements. Since the antenna mainly radiates in the region of θ= 0°-90° and ϕ= 180°-360° (see Fig. 19 (b)), the blue transition cable and pink metal platform in Fig. 19 (b) have very limited impacts on the measured results. The comparisons between the simulated and measured 3-D radiation gain patterns at 28.5 GHz are shown in Fig. 21. In general, the measurements are very similar to the simulations, but the measured data are a little noisier. The realized gain in different states is also measured and presented in Fig. 22. The gain is high in different states. Similar to the S parameters, the measured gain also shift slightly to higher frequencies. In addition, the measured gain is around 0.5 dB higher than the simulations, which may be due to the accuracy of the measurement setups.

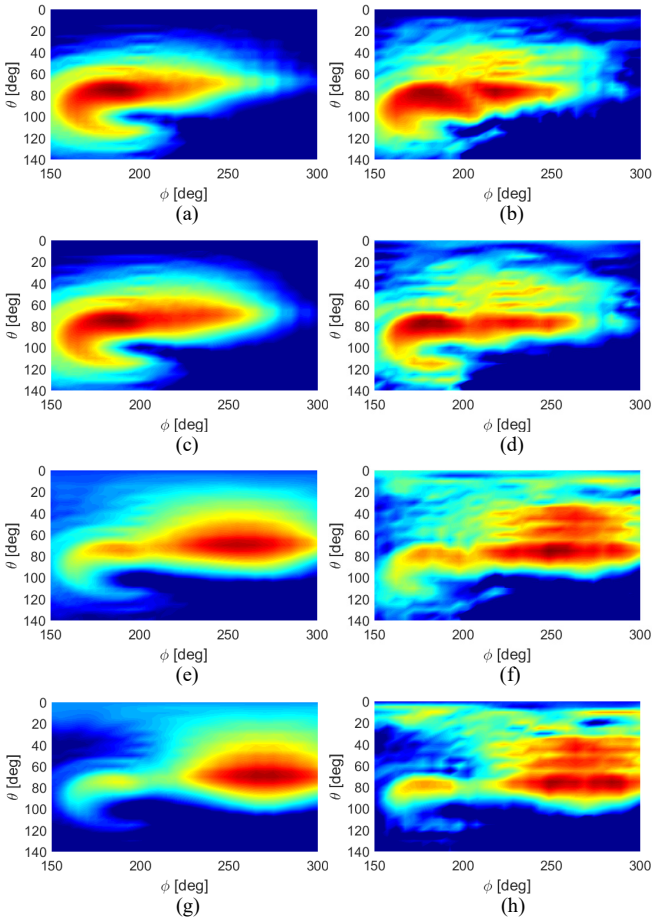

Fig. 21. Simulated 3-D radiation gain patterns of: (a) State A, (c) State B, (e) State C, and (g) State D; measured 3-D radiation gain patterns of: (b) State A(d) State B, (f) State C, and (h) State D. (The color bar is same to that in Fig. 8)

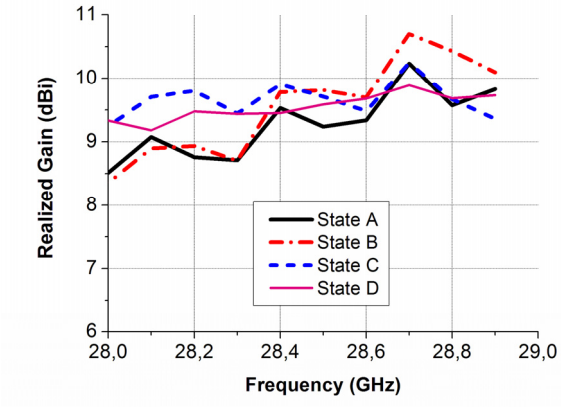

Fig. 22. Measured realized gain in different states at different frequencies.

The total scan pattern and coverage efficiency are also obtained based on the measured 3-D radiation patterns. They

are shown in Fig. 8 (b) and Fig. 9, respectively. As expected, the total scan pattern with the measured data is similar to that with the simulated. The coverage efficiency with the measurements agrees well with the simulated with threshold gain higher than 3 dBi. Between the threshold gain of -1 dBi to 3 dBi, the measured result is higher than the simulated due to the nosier measured radiation patterns.

VII. Conclusions

In this paper, a compact beam-steerable antenna array has been designed for 5G mobile terminals at 28 GHz. Two passive parasitic elements have been applied, which are loaded by short-circuited transmission lines of different lengths. By switching among different short-circuited transmission lines, the radiation pattern of one active element has been scattered to different directions. The impacts of switch loss have been analyzed. Two switches with 2.8 dB loss causes less than 1.82 dB loss for the whole array. The length of the whole array is less than 0.81 wavelength. The array has covered the band of 28-29 GHz with the scan angle larger than -90^o to 90^o. Two compact arrays have been placed on each long edge of the chassis and 360-degree beam steering has been achieved. The surface currents on the chassis of a mobile terminal have been utilized in order to obtain high gain for the small array. One more example has been added to show how to use the proposed method for planar antenna designs with high gain. Measurements have been carried out to verify the simulations. In general, all the measured results have good agreement with the simulations.

Acknowledgment

The authors would like to thank Peter Boie Jensen, Jesper Dejgaard Pedersen, and Ben Krøyer at Aalborg University for their help on the prototype fabrications.

References

[1] T. S. Rappaport, S. Sun, R. Mayzus, H. Zhao, Y. Azar, K. Wang, G. N. Wong, J. K. Schulz, M. Samimi, and F. Gutierrez, "Millimeter wave mobile communications for 5G cellular: It will work!," *IEEE Access*, vol. 1, pp. 335–349, 2013.

[2] T. Bai, and R. Heath. "Coverage and rate analysis for millimeter wave cellular networks," *IEEE Trans. Wireless Commun.*, vol.14, no. 2, pp. 110-1114, 2015.

[3] M. Nair, Q. Z. Ahmed, and H. Zhu, "Hybrid digital-to-analog beamforming for millimeter-wave systems with high user density," *IEEE Global Com. Conference (GLOBECOM"16)*, Dec. 2016.

[4] O. Alluhaibi, Q. Z. Ahmed, C. Pan, H. Zhu, "Capacity maximisation for hybrid digital-to-analog beamforming mm-wave systems," *IEEE Global Com. Conference (GLOBECOM"16)*, pp. 1-6, 2016.

[5] K. Zhao; J. Helander; D. Sjoberg; S. He; T. Bolin; Z. Ying, "User Body Effect on Phased Array in User Equipment for 5G mm Wave Communication System," *IEEE Antennas Wireless Propag. Lett.*, vol. 16, pp. 864-867, Sep. 2016.

[6] I. Syrytsin, S. Zhang, G. Pedersen, K. Zhao, T. Bolin, and Z. Ying, "Statistical investigation of user effects on mobile terminal antennas for 5G Applications," *IEEE Trans. on Antennas Propag.*, 2017. (In press)

[7] W. Hong, K. H. Baek, Y, Lee, Y, Kim, S. T. Ko, "Study and prototyping of practically large-scale mmWave antenna systems for 5G cellular devices," *IEEE Commun. Mag.*, vol. 52, no. 9, pp. 63-69, Sep. 2014.

[8] S.-J. Park, D.-H. Shin, and S.-O. Park, "Low side-lobe substrate-integrated-waveguide antenna array using broadband unequal feeding network for millimeter-wave handset device", *IEEE Trans. on Antennas Propag.*, vol. 64, no. 3, pp. 923-932, Mar. 2016.

[9] Y. Hou, X. Dong, and W. Xu, "5G cellular user equipment: from theory to practical hardware design," *IEEE Access*, vol. 5, pp. 13992-14010, 2017.

[10] J. Helander, K. Zhao, Z. Ying, and D. Sjoberg, "Performance analysis of millimeter wave phased array antennas in cellular handsets," *IEEE Antenna Wireless Propag. Lett.*, vol. 15, 2016.

[11] N. Ojaroudiparchin, M. Shen, S. Zhang, and G. F. Pedersen, "A switchable 3D-coverage phased array antenna package for 5g mobile terminals," *IEEE Antenna Wireless Propag. Lett.,* vol. 15, pp. 1747-1750, 2016.

[12] S. Zhang, X. Chen, I. Syrytsin, and G. F. Pedersen, "A planar switchable 3D-coverage phased array antenna and its user effects for 28 GHz mobile terminal applications" *IEEE Trans. Antennas Propag.* 2017. (In press)

[13] Q. L. Yang, Y. L. Ban, K. Kang, C. Y. D. Sim, G. Wu, "SIW multibeam array for 5G mobile devices," *IEEE Access*, vol. 4, pp. 2788-2796, Jun. 2016.

[14] Y. J. Cheng et al., "Substrate integrated waveguide (SIW) Rotman lens and its Ka-band multibeam array antenna applications", *IEEE Trans. Antennas Propag.*, vol. 56, pp. 2504-2513, Aug. 2008.

[15] Y. J. Cheng, Y. Fan, "Millimeter-wave miniaturized substrate integrated multibeam antenna", *IEEE Trans. Antennas Propag.*, vol. 59, pp. 4840-4844, Dec. 2011.

[16] Y. W. Hsu, T. C. Huang, H. S. Lin, Y. C. Lin, "Dual-polarized quasi Yagi-Uda antennas with end-fire radiation for millimeter-wave MIMO terminals," *IEEE Trans. on Antennas Propag.*, 2017. (In press)

[17] W. Hong, K. Baek, and S. Ko, "Millimeter-wave 5G antennas for smartphones: overview and experimental demonstration," *IEEE Trans. on Antennas Propag.*, 2017. (In press)

[18] R. F. Harrington, "Reactively controlled directive arrays", *IEEE Trans. Antennas Propag.*, vol. 26, no.3, pp. 390-395. May 1978.

[19] R. Vaughan, "Switched parasitic elements for antenna diversity," *IEEE Trans. Antennas Propag.*, vol. 47, no. 2, pp. 399–405, Feb. 1999.

[20] O. N. Alrabadi, J. Perruisseau-Carrier, and A. Kalis, "MIMO transmission using a single RF Source: Theory and antenna design," IEEE Trans. Antennas Propag., vol. 60, no. 2, pp. 654–64, Feb. 2012.

[21] D. Liu, X. Gu, C. W. Baks, and A. Valdes-Garcia, "Antenna-in-package design considerations for Ka-band 5G communication applications," *IEEE Trans. on Antennas Propag.*, 2017. (In press)

[22] Hubersuhner MMPX connector: https://www.hubersuhner.com/en/company/media/news/1015

[23] B. Yu, K. Yang, and G. Yang. "A novel 28 GHz beam steering array for 5G mobile device with metallic casing application." *IEEE Trans. Antennas Propag.* 2017. (In press)

[24] HMC1084: www.analog.com/en/products/rf-microwave/rf-switches/spst-spdt-sp3t-sp4t-sp6t-sp8t/hmc1084.html#product-overview

[25] ADRF5045: www.analog.com/en/products/rf-microwave/rf-switches/spst-spdt-sp3t-sp4t-sp6t-sp8t/adrf5045.html

[26] MAPS-010146: eu.mouser.com/new/macomtech/macommaps/

[27] QPC1000: www.qorvo.com/products/p/QPC1000